JOURNAL OF THERMOPHYSICS AND HEAT TRANSFER
Vol. 9, No. 4, October–December 1995

Mass Spectrometric Investigation of High Enthalpy Plasma Flows

Anja Schönemann* and Monika Auweter-Kurtz†
University of Stuttgart, 70550 Stuttgart, Germany

At the Institute for Space Systems three plasma wind tunnels for the simulation of conditions encountered by space vehicles during planetary entry are available. Two of these tunnels are equipped with a magnetoplasmadynamic accelerator, specially designed for the use of gas mixtures such as N_2/O_2 and carbon-containing gas mixtures. A quadrupole mass spectrometer that is placed inside the plasma jet is used to determine the plasma composition, the radial and axial distributions of all neutral and ionized particles, as well as the ion energy distributions. A theoretical investigation of the influence of the orifice opening on the sampling of radicals leads to a correction factor, with which the effect of recombination losses inside the orifice can be estimated. Additionally, a model of the space charge sheath in front of the orifice yields an equation for the evaluation of the ion temperatures. Different plasma conditions at ambient pressures of 0.1–2.9 mbar and at specific enthalpies of 19–33 MJ/kg were investigated.

Nomenclature

a = velocity of sound
c = concentration
c_p = heat capacity
D = diffusion coefficient
d = diameter of orifice opening
E = energy, electric field strength
e = elementary charge
f = degree of freedom
I = intensity
J_n = Bessel functions of first kind and nth order
K = dimensionless parameter of gas phase reactions
k = reaction rate constant
k_B = Boltzmann constant
L = length of orifice opening
L_A = Avogadro number
l = length
M = molecular weight
Ma = Mach number
m = mass
n = particle number density
p = pressure
R = radius
r = radial coordinate
T = temperature
U = voltage
v = flow velocity
$\bar{v}$ = mean thermal velocity
x, y, z = Cartesian coordinates
α_i = ith root of the Bessel functions $J_0(\alpha_i) = \alpha_i \delta J_1(\alpha_i)$
γ, γ' = recombination coefficient
δ, δ' = dimensionless parameter of catalycity
λ_D = Debye length
λ_i, λ_n = mean free path of ions, neutrals, respectively
ρ = density
υ = dimensionless parameter of velocity
Ψ = mole fraction

Subscripts
e = electron
f = floating
i = ion
M = molecule
ms = mass spectrometer
n = neutral
p = presheath
s = stagnation point
st = static
tot = total
0 = starting parameter
∞ = ambient

Introduction

THREE plasma wind tunnels[1–4] were built at the Institut für Raumfahrtsysteme (IRS) of the University of Stuttgart for the simulation of re-entry conditions with high specific enthalpies and low pressures as required for the development of modern oxidation-protected materials for the thermal protection of spacecraft.[5] The wind tunnels are connected to a power supply of 6 MW and a roots pump vacuum system with a total suction power of more than 250,000 m³/h. Two wind tunnels are equipped with a continuously operating magnetoplasmadynamic (MPD) accelerator, designed for power levels up to 0.5 MW and for specific enthalpies ranging from 5 MJ/kg to more than 150 MJ/kg. The stagnation pressure reaches from 0.1 mbar up to 50 mbar. The maximum mass flow rate is about 30 g/s.

The MPD accelerator that is used to create the plasma jet (see Fig. 1) consists of a cathode made of thoriated tungsten and an anode that forms the last segment of a water-cooled copper Laval nozzle. Inert gases like N_2, H_2, and Ar can be fed in along the cathode, which glows during operation, giving a very low cathode erosion rate, while oxidizing gases like O_2 are injected with high radial velocity just behind the nozzle throat. At high mass flow rates and low power levels a protective gas layer of argon is injected tangentially at the anode for a N_2/O_2 flow.

Different well-known experimental methods are applicable for the investigation of the plasma conditions.[1,3,5–7] At the IRS pitot, heat flux, catalytic,[8,9] and electrostatic probes,[10] as well as emission spectroscopy[11] and Fabry–Perot interferometry[12] are used, and thus, they can be applied for comparison and in addition to the mass spectrometer. All probes are mounted on a platform with four motor-driven axes. Three

Received Sept. 30, 1994; revision received Jan. 23, 1995; accepted for publication Jan. 24, 1995.

*Dr.-Ing., Scientist, currently at Laboratoire d'Aérothermique du CNRS, 4ter route des Gardes, 92190 Meudon, France. Member AIAA.
†Professor, Aerospace Engineering. Member AIAA.

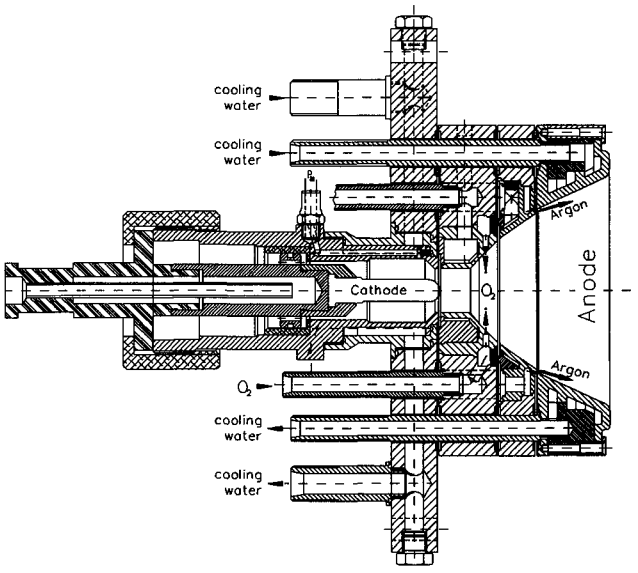

Fig. 1 Schematic of the MPD-generator RD5-IRS.

of these axes are linearly oriented, axial, radial and vertical to the plasma jet axis, the fourth one provides the possibility to rotate the probes. Due to its dimensions the mass spectrometer is only movable in the x and y direction.

Mass Spectrometer

The mass spectrometer used here is based on a VG Quadrupole[13] SXP300/CMA500 and consists of an open electron impact ion source, a cylindrical mirror energy analyzer (CMA, 0–50 eV), a triple filter quadrupole (0–300 amu), and a channeltron (see Fig. 2). In front of the ion source an ion transfer optic (ITO) is installed, a small aperture lens, with which external ions can be focused into the CMA while the ion source is switched off. In the case where neutrals are detected, a reflecting potential for positive ions is applied to the ITO and the ion source is switched on. Thus, mass scans at a constant energy and energy scans at a constant mass can be carried out for neutral as well as ionized plasma particles.[14]

The mass spectrometer is situated inside the vacuum chamber of the plasma wind tunnel. Therefore, the whole spectrometer housing is protected by a water-cooled copper heat shield against the high heat loads and the erosive environment. All equipment is placed outside the vacuum chamber, i.e., the electrical support is made through a flexible tube under atmospheric pressure while the vacuum support is done with a CF100 bellow, which also serves the movability of the spectrometer.

The spectrometer head, which is shown in Fig. 3, contains the orifice opening (diameter 100 μm, length 100 μm), drilled into a tungsten plate (diameter 39 mm, thickness 4 mm) with an eximer laser, and additionally, the special orifice cooling body. The spectrometer head is electrically insulated from the rest of the housing, thus, the orifice is floatable. In case of high pressures (>1 mbar) a tungsten foil instead of the tungsten plate is used yielding again a length-to-diameter ratio for the orifice of $L/d = 1$ for all measurements (opening diameter 40 μm). For comparison, an orifice ratio of $L/d = 2$ was also used. The orifice opening serves also as a one-staged differential pumping system.

The ITO is placed 32 mm behind the orifice opening. Long paths inside the spectrometer leading to particle losses are avoided. The spectrometer was calibrated with neutrals, external atoms, and external ions to show the function and accuracy of the CMA for energy analysis, the relative sensitivities of the spectrometer for different masses, and to demonstrate the influence of the orifice opening on the sampling

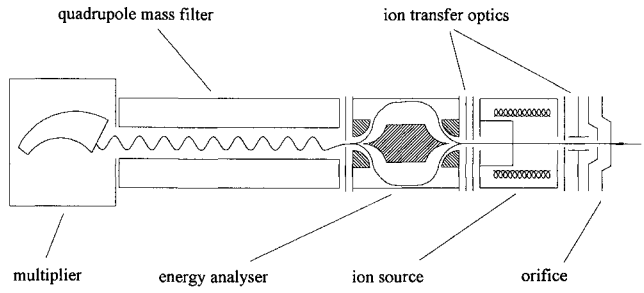

Fig. 2 Schematic of the mass spectrometer.

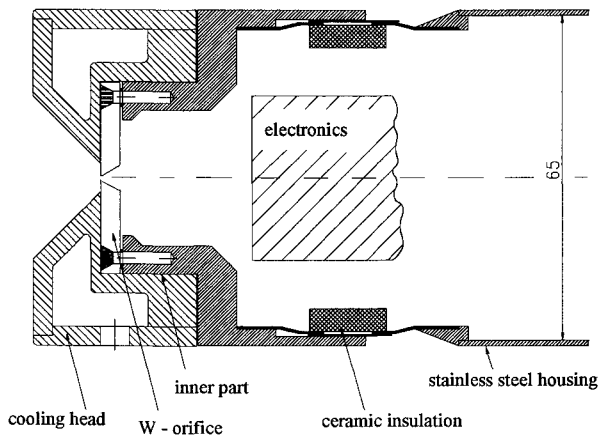

Fig. 3 Schematic of the spectrometer head with orifice opening.

of atoms and ions as well as the influence of a space charge sheath in front of the orifice on the measured ion energies.[15]

The CMA was shown to measure with an error of ± 0.5 eV in the relevant energy region of 0–50 eV. The normal fluctuation of the signal within an energy scan of a neutral particle is around 10%. In contrast, it was observed that for plasma ions, which have a very high intensity (e.g., N^+ with up to 10^6 counts/s), these fluctuations can increase to 20%. The mass resolution of the quadrupole is set to $\Delta m/m = 1$, i.e., neighbored masses like water ($m = 17, 18$) can be resolved, but not that of certain molecules like N_2 and CO ($m = 28$). To distinguish between molecules with the same mass number and to distinguish between radicals that were produced inside the plasma and enter the spectrometer and those that were produced inside the ion source, the particles' ionization potentials can be used.[16] Therefore, the electron impact energy of the ion source was lowered from 70 eV down to 17 eV. Here, dissociation of a molecule, e.g., O_2, and subsequent ionization of the fragment, O, is not possible. Thus, O-atoms detected inside the plasma jet at this electron energy can entirely be attributed to the plasma. Additionally, a reference spectrum of the residual gas inside the spectrometer can easily be subtracted from the data taken inside the plasma jet.

Sampling of Atoms

The sampling of radicals is mainly governed by the dimensions of the orifice opening, its material, and the rate of transport inside the opening. Additionally, the stagnation point has to be taken into account for the loss of atoms and ions due to recombination reactions.

A very simple theory describing the losses inside the orifice opening is given by Helm.[17] Here, the particles diffuse through a cylindrical channel where molecular flow conditions hold. At the walls total reflection is considered while a temperature or pressure dependence is not taken into account. The part of undisturbed particles passing through the orifice channel is thus given by the Clausing factor,[17] which corresponds to the flow resistance of a neutral gas inside a short tube. The

correction factor for an orifice with a dimension ratio of $L/d = 1$ is 0.514, i.e., 51.4% of the particles are sampled without any disturbance. In the case where $L/d = 2$, the factor is already 0.359.

A complete description of a convective flow through a cylindrical orifice channel including gas phase reactions, catalytic wall reactions, and diffusion was given by Wise and Ablow.[18,19] The common theory can be solved numerically only for special cases, but two analytical solutions can be found if some simplifications are considered. At first, some rigid assumptions are made: no convective flow, no wall catalycity, and no gas phase reactions. This leads to the simple differential equation[18]

$$D \frac{\partial^2 n}{\partial z^2} = 0 \tag{1}$$

with a solution for the ratio of particles n at length L of the orifice opening to the particles n_0 in front of it

$$\left(\frac{n}{n_0}\right)_L = \frac{\delta'}{\delta' + 2L/d} \tag{2}$$

Here, δ' is a dimensionless parameter describing the catalycity of the detection system ($\gamma' = 1$, i.e., all particles will be detected) with

$$\delta' = \frac{8D(1 - \gamma'/2)}{\bar{\nu}\, d\gamma'} \tag{3}$$

Thus, the solution is dependent not only on the orifice's dimension ratio (like the solution for the theory of Helm), but also on the diffusion coefficient D of the radicals in their neutral gas and on the thermal velocity, i.e., a temperature and pressure dependence exists.

A second, not so rigorous assumption is to take only homogeneous reactions in the gas phase into account. This leads to the differential equation[19]

$$D \frac{\partial^2 n}{\partial z^2} - v \frac{\partial n}{\partial z} - knc_M^2 = 0 \tag{4}$$

with the common solution, if no radial dependence of the particle distribution inside the orifice opening exists

$$\frac{n}{n_0} = 2 \exp[v(\lambda - \zeta)] \sum_{i=1}^{\infty} \frac{f_i(\zeta) J_0(2\alpha_i r/d)}{\alpha_i(1 + \delta^2\alpha_i^2) f_i(\lambda) J_1(\alpha_i)} \tag{5}$$

Here the following parameters are used for abbreviation:

$$\zeta = 2\frac{L - z}{d}, \qquad v = \frac{vd}{4D} \tag{6a}$$

$$\lambda = \frac{2L}{d}, \qquad K = \frac{kc_M^2 d^2}{4D} \tag{6b}$$

$$f_i = \sinh \beta_i\zeta + \delta'(\beta_i + v)\cosh \beta_i\zeta - \delta' v \exp(-\beta_i\zeta) \tag{6c}$$

$$\beta_i = (v^2 + K^2 + \alpha_i^2)^{1/2} \tag{6d}$$

δ is the dimensionless parameter of the wall catalycity, defined analogous to Eq. (3) with the catalytic recombination coefficient γ of the walls. Averaging over the opening area for small α, assuming that $\delta >> 1$, and therefore, $\alpha_1 \cong \sqrt{2/\delta}$, while all other elements of the summation vanish, and evaluating $f(\zeta = 0) = \delta'\beta_i$, yields the solution for this approximation at length L of the orifice opening

$$\left(\frac{n}{n_0}\right)_L \cong 4 \exp(v\lambda) \frac{2\delta'\beta_1}{2/\delta(1 + 2\delta)} \times \frac{1}{[\delta'(\beta_1 - v) - 1]\exp(-\beta_1\lambda) + [1 + \delta'(\beta_1 + v)]\exp(\beta_1\lambda)} \tag{7}$$

Table 1 Calculated diffusion coefficients and particle ratios for a tungsten orifice with $L/d = 1$

p, mbar	T, K	D_{N,N_2}, 10^{-4} m²/s	$(n/n_0)_L$, Eq. (2)	$(n/n_0)_L$, Eq. (7)
0.1	300	3812	0.950	0.920
1.3	300	293	0.500	0.450
——	1500	4274	0.850	0.848
2.9	300	131	0.280	0.230
——	1500	1916	0.720	0.718
——	3000	6035	0.858	0.856

Now, a calculation of $(n/n_0)_L$ for a tungsten orifice with $L/d = 1$ at different plasma conditions can be worked out. Therefore, the diffusion coefficient of N atoms in their neutral gas N_2 was calculated with the Chapman–Enskog theory.[20] In Table 1 the diffusion coefficients and the particle ratios calculated with Eqs. (2) and (7) are listed for the plasma conditions that were investigated in the plasma wind tunnel at different particle temperatures. The flow velocity was estimated with the effective pumping speed at the orifice opening, giving $v = 13.8$ m/s in the worst case (i.e., lowest acceptable suction power of the turbopump yielding a maximum pressure of $\leq 1 \times 10^{-5}$ mbar inside the spectrometer) and a resident time of 7.2 μs for the particles inside the orifice channel. The reaction rate constant k_{NN} was estimated with the Park[21] air chemistry model. The concentration of the molecules can be calculated with

$$c_M = p/k_B T L_A \tag{8}$$

Since the mole fraction of the radicals was considered to be very small in comparison with that of the molecules, and since the rate constant k_{NN} was defined for the homogeneous recombination reaction of two N atoms to a N_2 molecule, Eq. (6b) for K additionally has to be multiplied with the mole fraction Ψ_N of the atoms.

There are now three major conclusions: 1) the higher the temperature for a given pressure, the higher the particle flow of radicals through the orifice; 2) at lowest pressure, even at room temperature, already 92% of the radicals pass the orifice; and 3) both approximations give nearly the same percentage of radicals sampled with the orifice. As a result, the assumption of a noncatalytic wall, an absence of gas phase reactions and convective flow inside the orifice channel, like for the theory of Helm, holds for the existing orifices. Also, since the temperature of the sampled particles inside the orifice channel is not known, for simplification the theory of Helm was applied as a correction factor for the high-pressure test cases. Obviously, at low pressures a correction factor is not necessary.

The complete theory was also applied by Willey and Blake[22] to a sampling system of $2L/d \approx 400$ (a four-staged differential pumping system), with the result that even here gas phase reactions could be neglected at low pressures, but catalytic wall reactions and convective flow had to be taken into account.

Sampling of Ions

The sampling of ionized plasma particles is inevitably disturbed by the plasma sheath generated in front of a probe that is placed into the plasma. In accordance with the kind of plasma and the dimensions of the probe, a theory describing the sheath has to be applied. Due to the dimensions of the probe and the plasma parameters of the investigated high-enthalpy plasma flows,[8,14,23] the following relations hold: 1) $\lambda_i/\lambda_D >> 1$, resulting in a collisionless plasma sheath (λ_i in mm, λ_D in μm); 2) $R_{ms} >> \lambda_D$, yielding a planar plasma sheath; 3) $\lambda_n, \lambda_i > d > \lambda_D$, i.e., no disturbance of the velocity distribution of charged particles by sampling through the orifice; 4) $\lambda_D < d$, i.e., the space charge sheath "sees" the orifice

opening, a small curvature is expected; and 5) d/λ_i, $d/\lambda_n < 1$, giving molecular flow inside the orifice.

The plasmaphysical model assumes a positively charged space-charge sheath and a quasineutral presheath in front of it, which originates from the Bohm criterium.[24] The space charge region can be considered as a thin (a few electron Debye lengths thick) collision-free planar sheath. The presheath extension can be assumed to be in the order of a mean free path (a few millimeters).[24] The potential developed by the space charge sheath is estimated with the ordinary Langmuir theory. Taking into account that distributions of ion masses, electron temperatures, and densities are measured inside the plasma jet at a given position, the potential over the space charge sheath of the floating probe is given by

$$U_{st}(x, y) = \frac{1}{2}\frac{k_B T_e(x, y)}{e} \ln\left[\frac{T_e(x, y)}{\bar{T}_i(x, y)}\frac{\bar{m}_i(x, y)}{m_e}\right] \quad (9)$$

with a mean ion mass at a position (x, y) of

$$\bar{m}_i(x, y) = \sum \Psi_i(x, y) m_i \quad (10)$$

and a mean ion temperature $\bar{T}_i$.

The space charge sheath potential is reduced by the potential over the presheath. The presheath potential U_p can be estimated with the ion current reaching the plasma sheath edge as a result of the ion drift inside the electrical field, which arises from the presheath, with the electrical field at the sheath edge given by[24]

$$E_0 = \frac{k_B T_e}{e\lambda_D^{2/5} l_p^{3/5}} \quad (11)$$

with the characteristic length l_p for the presheath, and the continuity equation for the charged particle density in a planar field.[25] This leads to the following expression for the presheath potential:

$$U_p(x, y) = \frac{1}{2}\frac{k_B T_e(x, y)}{e} \ln\left[\frac{\pi}{4}\frac{T_e(x, y)}{\bar{T}_i(x, y)}\frac{\lambda_i(x, y)}{\lambda_D^{2/5}(x, y) l_p^{3/5}}\right] \quad (12)$$

The measured floating potential U_f of the insulated probe is now given by the difference of both potentials:

$$U_f(x, y) = U_{st}(x, y) - U_p(x, y) \quad (13)$$

Additionally, the measured ion energies can be assumed to be equivalent to the sum of both potentials. When the ions reach the plasma sheath, their velocity has been reduced down to a value of about zero due to the stagnation point in front of the orifice. The kinetic energy can be neglected in comparison with the energy the ions gain inside the sheath. The ion energy E_i is then given by

$$E_i(x, y) = e[U_{st}(x, y) + U_p(x, y)] \quad (14)$$

A summation of these two equations leads to an expression for the charged particle temperature in front of the orifice under the assumption of thermal equilibrium in the stagnation point and singly charged ions.[15,23] A validation of the so-determined ionized particle temperatures was presented in Ref. 23. Here a comparison between the temperature gained with electrostatic probes, which were situated in the mass spectrometer's cooling head some mm in front of the orifice opening, and the average ion temperature calculated with the ion energies of all species was carried out.

Test Case at 0.1-mbar Ambient Pressure

The plasma conditions for this test case are 0.1-mbar ambient pressure, a current of 1000 A, 1 g/s N_2, 0.25 g/s O_2, and 0.3 g/s Ar as anode protection gas leading to an average specific enthalpy of 28 MJ/kg at the end of the MPD generator and a total pressure of 0.56 mbar in the center of the plasma jet. A 100-μm orifice with $L/d = 1$ was used and, as explained above, no orifice correction factor was applied. Measurements of the radial distributions of neutral and ionized particles at distances of 260 and 330 mm to the anode were carried out.

Since the energy scan of neutral particles is likely to show the energy distribution of the particles gained inside the ion source, the neutrals are detected independent of their temperature inside the plasma jet. This allows for a calibration of the neutrals before a measurement is made inside the plasma wind tunnel, which directly yields the neutral partial pres-

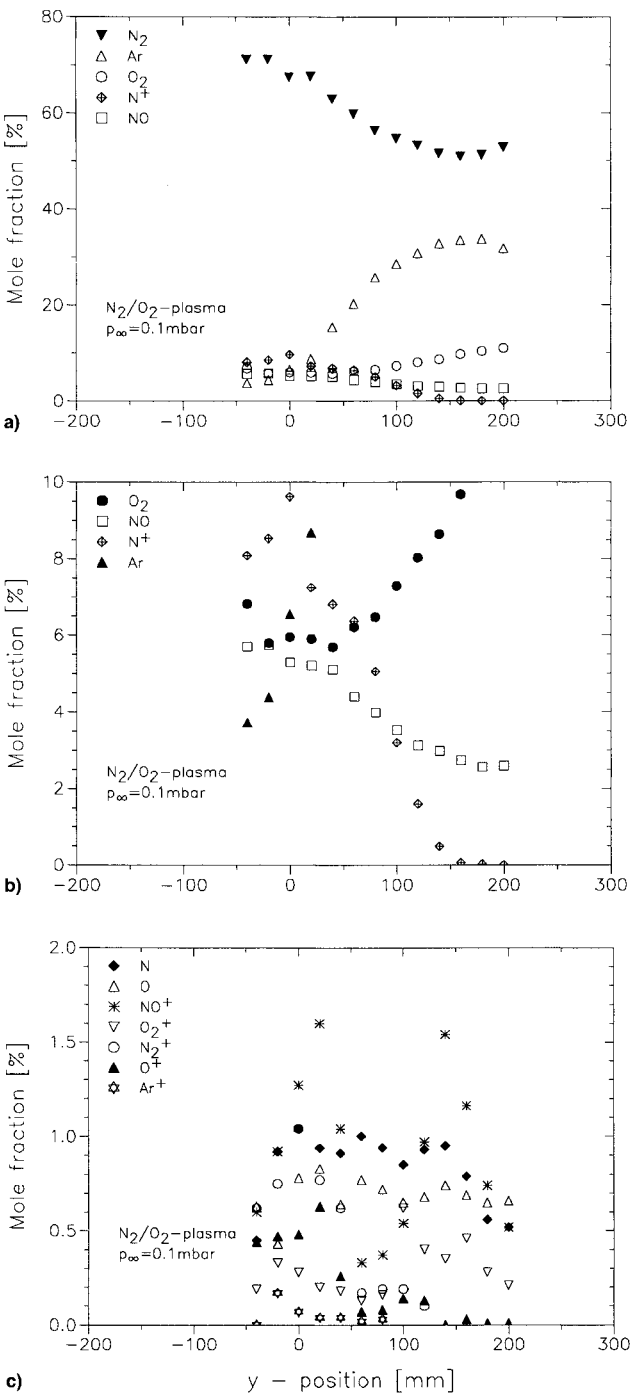

Fig. 4 Total radial partical distribution in a N_2/O_2 plasma at 0.1 mbar and x = 260 mm (uncertainty 20–25%). Ordinate scale a) 0–80%, b) 0–10%, and c) 0–2%.

sures. Considering a local thermodynamic equilibrium, the neutral particle densities can be evaluated by

$$n_n(x, y) = \frac{k_B T_n(x, y)}{p_n(x, y)} \tag{15}$$

The determination of the neutral particle temperature will be explained as follows.

It is not possible to calibrate external ions inside the plasma wind tunnel. However, taking into account that only singly ionized particles are present, an ion particle density can be evaluated with the electron density measured by electrostatic probes[10] and with the ion mole fraction determined with mass spectrometry

$$n_i(x, y) = \Psi_i(x, y) n_e(x, y) \tag{16}$$

Thus, a total particle distribution can be worked out (see Figs. 4a–4c). The main component in the center and at the border of the plasma jet is N_2. In the center of the jet it is followed by N^+, O_2, NO, and Ar; the amounts of all other components like NO^+, N, O, and N_2^+ are smaller than 2%, while those of O^+, O_2^+, and Ar^+ are less than 1%. At the border of the plasma jet N_2 is followed by Ar, which was mixed in at the anode with an amount of about 20% of the total mass flow rate, O_2, NO, NO^+, and O_2^+, and a small amount of N and O. At the edge of the plasma jet only molecular ions containing oxygen are present. The oxygen that was mixed into the jet in the supersonic part of the nozzle[1,5] (see Fig. 1) shows a nearly constant distribution over the plasma jet, while the anode protection gas Ar is mainly present at the plasma jet border for this low pressure. The amount of atomic neutral particles like N and O is very low especially compared to N_2 and N^+. This indicates a high chemical nonequilibrium in the plasma jet. The fact is also supported by a numerical simulation of the chemical composition for these plasma conditions yielding a time constant of >100 s for the plasma to reach chemical equilibrium. A small amount of N_2O^+ ions was found in the center of the jet (<<1%), which is not depicted in Fig. 4, but no NO_2 was produced at these plasma conditions. There was no indication for doubly-charged particles. The error of the mass-spectrometric measurements can be assumed to be 10–15% (see above). The error sums up to a total of 20–25%, if all other measurement techniques used to calculate the distribution are also considered.

In contrast to the energy distribution of the neutrals the ion energy distribution is not affected by any ion source and, therefore, resembles the distribution of the ions gained inside the plasma and in the plasma sheath in front of the orifice. It is therefore necessary to carry out an energy scan for each ion at each position inside the plasma jet. The energy distributions of all ions are quite similar. In Fig. 5, as an example, the ion energy distribution for O_2^+ ions at two different radial positions y = 140 and 60 mm at a distance of 330 mm to the anode are shown. As expected, the intensity of the ions increases inside the jet, but also the energy maxima are shifted to higher values and, surprisingly, two maxima are present at the border of the plasma jet while in the center a third occurs (see Fig. 6). These multiple, distinct energies were observed for all kinds of ions, molecular and atomic, at each position inside the plasma jet. Only at that position, where the splitting into three maxima takes place, it was sometimes difficult to distinguish between these two maxima. Even the energies are quite the same for all ions independent of the different places of their production, like for O_2^+ and N^+ (see Fig. 6).

The two maxima at the border can be explained easily; since the ions are accelerated and heated thermally inside the nozzle and additionally by the MPD forces of the arc, they gain a higher temperature than the neutrals. Thus, the higher energy maximum at the border of the plasma jet corresponds

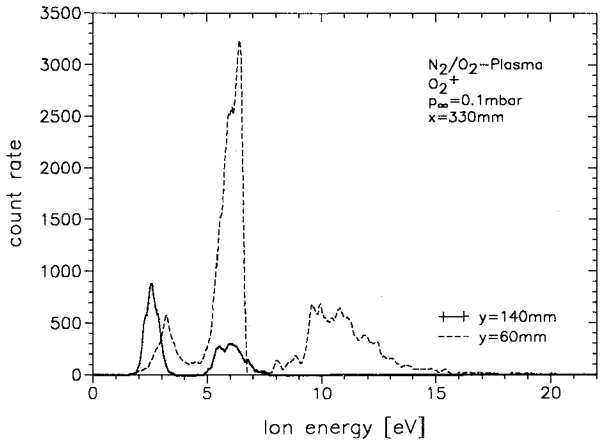

Fig. 5 Energy distribution of O_2^+ at y = 140 and 60 mm and at a distance of x = 330 mm to the anode (uncertainty ±0.5 eV).

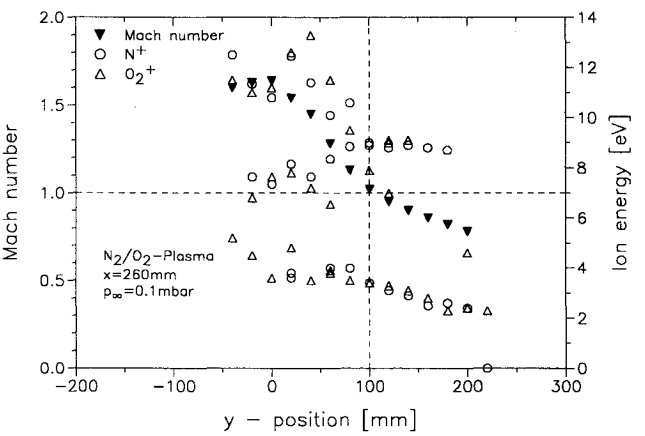

Fig. 6 Comparison of the Mach number with the energy distributions of the two different ions O_2^+ and N^+ (uncertainties: energy ±0.5 eV, Mach number 25%).

to those ions that were generated inside the plasma generator, while the lower energy maximum corresponds to those ions that were generated in charge transfer collisions between ions and neutrals and, therefore, resembles the energy of the neutral particles. The third maximum, which occurs in the center of the jet, can be explained by the following general considerations.

With Eqs. (13) and (14) (ion energy of the lowest energy maximum of all ions and floating potential), the average temperature of the neutrals T_n and, afterwards, the total particle distribution have been calculated (see Fig. 4). Now the mean number of degrees of freedom (DOF)

$$\bar{f}(x, y) = \sum_j \Psi_j(x, y) f_j \tag{17}$$

and the mean molar mass of the gas mixture

$$\bar{M}(x, y) = \sum_j m_j \Psi_j(x, y) \tag{18}$$

can be evaluated. With these two values the local specific heat capacity is given by

$$c_p(x, y) = \frac{\bar{f}(x, y) + 2}{2} \frac{R_G}{\bar{M}(x, y)} \tag{19}$$

and the adiabatic exponent can be estimated with[9]

$$\kappa(x, y) \cong \frac{c_p(x, y)}{c_p(x, y) - [R_G/\bar{M}(x, y)]} \tag{20}$$

The determination of the average ion temperature with Eqs. (13) and (14) (ion energy of the mean energy maxima of all ions and floating potential) now enables the calculation of the local speed of sound. The total particle density and the mean molar mass of the mixture give the local density, which together with the results of pitot probe measurements of the pressure inside the plasma lead to the local plasma velocity

$$v(x, y) = \sqrt{\frac{p_{tot}(x, y) - p_{st}}{\rho(x, y)}} \quad (21)$$

The static pressure was assumed to be equal to the ambient pressure of 0.1 mbar. Now the local Mach number can be calculated.

In Fig. 6 the Mach number distribution is shown together with the energies of two totally different plasma ions, namely, N^+ and O_2^+. The Mach number at the border of the jet is below 1, i.e., here the plasma jet is subsonic. Around y = 100 mm the plasma conditions change to supersonic conditions. Obviously, the lowest energy maximum (around 4 eV) is not affected except for an increase of the energy inside the plasma jet. The second energy maximum remains until y = 100 mm, where a splitting into two branches is observable. Thus, the third energy maximum can be explained by a supersonic shock in front of the orifice leading to an additional heating of a part of the ions, which appears at higher energies.

To prove the calculated Mach number, the stagnation pressure and temperature behind a stationary shock front were calculated with[26]

$$p = p_\infty \frac{(1 + \tilde{f})^{1+\tilde{f}} Ma^{2+\tilde{f}}}{\tilde{f}^{2+\tilde{f}/2}[(2 + \tilde{f})Ma^2 - 1]^{\tilde{f}/2}} \quad (22)$$

with

$$T = T_\infty[1 + (Ma^2/\tilde{f})] \quad (23)$$

and compared with the measurement results. In the center of the jet a mean DOF of 4.57 and a Mach number of 1.64 yield a stagnation pressure of 0.404 mbar, while the pitot probe measurements give 0.46 mbar. The temperature of the ions in the plasma freestream is calculated with the mean energy maximum T_∞ = 9500 ± 450 K. Equation (23) yields a temperature T of the ions due to the shock front of 15,090 K. The corresponding temperature calculated with the high-energy maxima is 14,500 ± 700 K. Taking into account all assumptions that were made for the calculation of the Mach number and with respect to the accuracy of the mass-spectrometric measurements, these results compare very well.

Thus, the mass spectrometric measurements at low pressure show that 1) only singly-charged ions are present; 2) the plasma velocity is supersonic; 3) the influence of the stagnation point on the plasma composition can be neglected for dilute gas mixtures; 4) ions and neutrals have different temperatures (T_n = 6500 K, T_i = 9500 K for x = 260 mm, y = 0 mm), i.e., at least three different temperatures exist T_e, T_i, and T_n (there is no information about the vibrational temperature); and 5) due to these three temperatures the plasma is in a high chemical nonequilibrium giving very low neutral atomic particle densities.

Test Case at 1.3-mbar Ambient Pressure

The plasma conditions examined within this test case[14,27] are at an ambient pressure of 1.3 mbar leading to a total pressure of 3 mbar in the center of the jet, a current of 1000 A and 1.0 g/s N_2 without anode protection gas. An average specific enthalpy of 33 MJ/kg is reached at the end of the anode. A 50-μm orifice with L/d = 2 was used for carrying out radial distributions of neutral particles at x = 260 and 330 mm.

As previously explained, an orifice correction factor has to be applied to the measured data. The pressure inside the spectrometer increased when the ambient pressure was raised to 1.3 mbar, suggesting that the orifice opening is too large for operation at this pressure level. Therefore, a correction was made to the measured values to account for the effect of high pressure. A residual gas species that is not affected by the plasma is measured additionally, e.g., H_2O. The radial distribution of H_2O should be a constant, except possibly for a small decrease in the center of the jet, where the temperatures are high and collisions between plasma particles and residual gas particles could occur. If this distribution is not constant, the surplus of the count rates in the center of the jet can be recalculated assuming the real H_2O-signal to be constant. In all cases, the signal of N was corrected by

$$I_N = (I_{o,N} - I_{p,N}) + 2 \cdot 0.641 \cdot x(I_{o,N_2} - I_{p,N_2}) \quad (24)$$

and N_2 correspondingly. Here, I_N is the real signal of the atoms, the index o gives the originally measured intensities, while p corresponds to the surplus intensities because of the pressure increase. The factor 0.641 arises in accordance with the theory of Helm for an orifice with L/d = 2, where the N atoms recombine inside the orifice channel to N_2 molecules, so that the two intensities sum up to the real molecular intensity I_{N_2}. All measurements, e.g., the temperature, show a strong radial distribution of the plasma parameters. Thus, the number of N atoms is not constant over the jet, but shows the same distribution as all other parameters. This was accounted for by the factor x, which is 0% at the border of the plasma jet and rises to 100% in the center. In Fig. 7 the three particle distributions are shown, at the top the original data (Fig. 7a), in the middle (Fig. 7b) the pressure-corrected data (here the signal of H_2O was assumed to be constant in the center), and at the bottom (Fig. 7c) the orifice-corrected, real particle distribution. In Fig. 8 the data so corrected are compared with a numerical simulation, which has been presented elsewhere in detail.[14,27] As seen in the figure, the mass-spectrometric data are in good qualitative and quantitative agreement with the theoretical predictions.

Radial distributions of ions could not be determined because a high recombination rate of the ions leads to very low count rates at the stagnation point and at a too high pressure inside the spectrometer. A few measurements have been made showing that the main component is N^+ arriving at an energy of 2.8 eV, which yields a temperature of 3564 K. This relatively low temperature shows that the ions have already cooled down in front of the orifice, but are far from the wall temperature of the orifice cooling head. Thus, again, the stagnation point is visible but can be neglected in a first approach and no "stagnation point" correction factor has to be applied to the data. This is also supported by the quantitatively good agreement shown in Fig. 8. Additionally, the single energy maximum of the ionized plasma particles indicates that the plasma conditions are subsonic and the temperatures of ions and neutrals are the same. This is also supported by the numerical simulation[14,27] and by the comparison with an analytically determined distribution that is based[9] on the results of heat flux, pressure, electron density, electron temperature, and velocity measurements, and from which the local mass fluxes and particle densities were calculated.[27]

Test Case at 2.9-mbar Ambient Pressure

The plasma conditions investigated here[8,9] were chosen to simulate the conditions that result in a maximum-calculated temperature at the leading edge at the re-entry of the space vehicle HERMES. The conditions are an ambient pressure of 2.9 mbar leading to a total pressure of 4 mbar in the center of the jet at x = 300 mm, 1.3 g/s N_2 without anode protection gas, and a current of 750 A. This results in an average specific enthalpy of 19 MJ/kg at the end of the anode. A tungsten foil

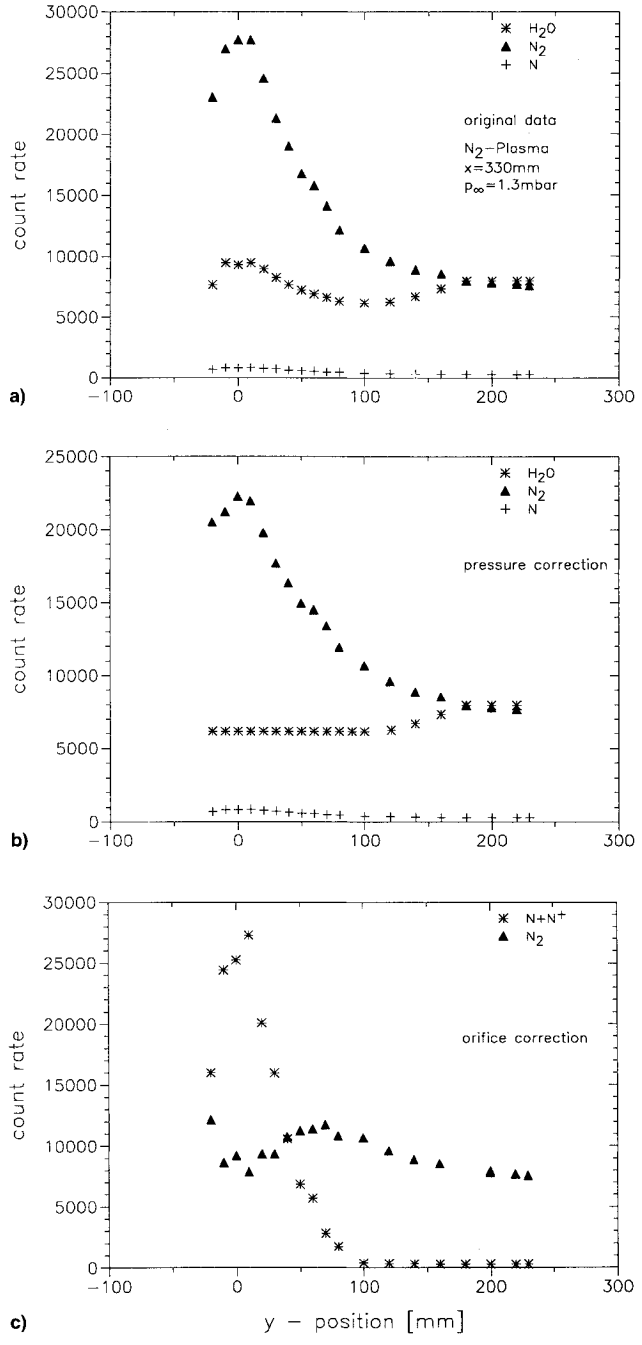

Fig. 7 Neutral particle distribution: a) original data, b) pressure correction, and c) orifice correction/real data.

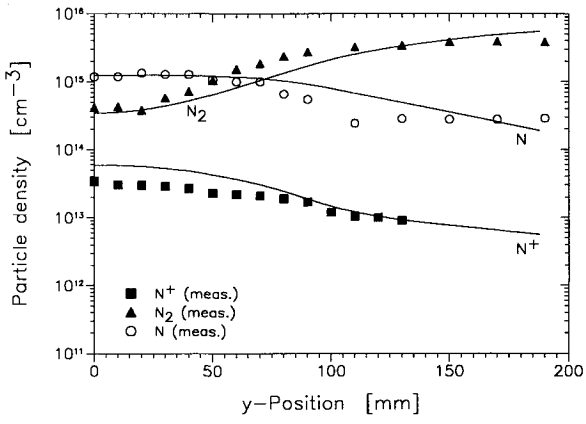

Fig. 8 Comparison of mass spectrometric data and results of the numerical simulation of the 1.3-mbar test case.[27]

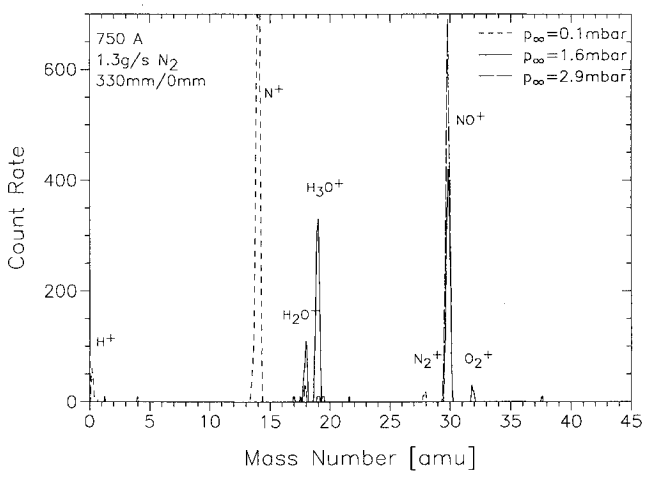

Fig. 9 Ion spectra taken at the plasma conditions of the 2.9-mbar test case, but at varying ambient pressure.

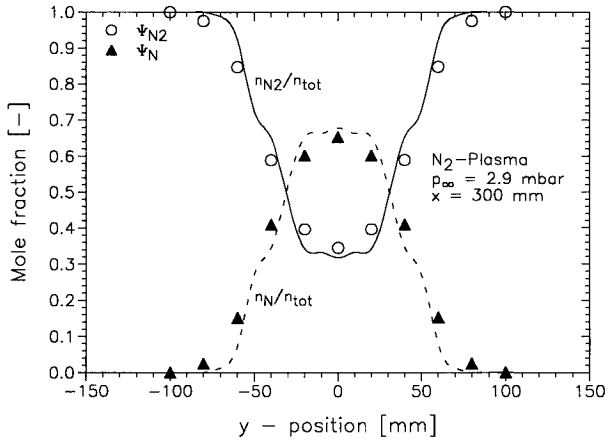

Fig. 10 Comparison of the neutral particle distribution determined by mass spectrometry (uncertainty 25%) and calculated analytically[8,9] (uncertainty 20–25%) for the 2.9-mbar test case.

with an opening diameter of 40 μm and $L/d = 1$ was used for the mass spectrometric measurements. Since the orifice opening has proved to be sufficiently small for the pressure conditions, no pressure correction had to be applied to the data. Accordingly, the orifice correction factor for an orifice with $L/d = 1$ was used.

Again, no radial distribution of ions in the plasma jet could be measured because the stagnation point causes a high recombination rate of the ions. A few measurements in the center of the jet surprisingly show that the only observable external ion entering the mass spectrometer is at mass 30, i.e., NO^+ (see Fig. 9). Since only nitrogen is fed in at the generator, this ion is definitely produced in front of the orifice due to associative charge transfer reactions of ionized plasma particles and residual gas particles, namely, N^+ and O_2 or H_2O. The ion energy is 0.8 eV, yielding a temperature of around 1500 K. Again, this temperature is too low for ions in the plasma freestream, but it is still much higher than the temperature of the cooled wall! As discussed, the influence of the stagnation point on the plasma composition is observable, but can still be assumed to be small. To elucidate the influence of the stagnation point on the measurement of ions, the 2.9-mbar test case conditions were chosen and, while the mass spectrometer was placed in the center of the jet, the ambient pressure was lowered to 0.1 mbar: In Fig. 9 three different ion spectra at 2.9-, 1.6-, and 0.1-mbar ambient pres-

sure are shown. At minimum pressure the main contribution is made by N^+ (there is a small amount of N_2^+). Already at 1.6 mbar this particle has disappeared and is displaced by NO^+ and residual gas components like H_2O^+, H_3O^+, and O_2^+. At the 2.9-mbar test case conditions these intermediate ions have nearly vanished and NO^+ is the main component.

In Fig. 10 the measured neutral particle distribution at $x = 300$ mm is compared with the analytically determined particle distribution.[9] The analytically determined distribution is based on the results of heat flux, pressure, electron density, electron temperature, and velocity measurements, from which the local specific enthalpy, ion temperatures, and vibrational temperature were evaluated or estimated and the local mass fluxes and particle densities were calculated.[9] When the previously mentioned influence of the stagnation point is taken into account, the error of the mass-spectrometric data has to be assumed to be around 25–30%. Since also the analytical particle distribution is based on measurement data whose errors also sum up to around 20–25%, it can be said that a very good agreement is obtained.

Discussion and Conclusions

The mass spectrometer with a planar orifice has proven to be a useful tool for the determination of the plasma composition and particle distribution up to a total pressure of 5 mbar. The experimental results show a qualitatively and quantitatively good agreement with the numerical simulation and with analytical calculations.

By describing the plasma sheath in front of the orifice correctly, ion temperatures can be obtained from the measured ion energies and the floating potential of the orifice. For low pressures ($p_\infty = 0.1$ mbar), these temperatures correspond to freestream conditions, whereas for the higher pressures the ions cool down in the stagnation region, but still have a much higher temperature than the orifice cooling head walls.

The simple theory of Helm for an orifice correction factor has proven to be sufficient to obtain reliable results for high pressures. From the complete theory of Wise and Ablow, a higher correction factor for the case with $p_\infty = 2.9$ mbar and $T_i = 1500$ K would be expected than for $p_\infty = 1.3$ mbar and $T_i = 3564$ K, because Table 1 indicated a higher percentage of atoms transmitted at higher temperatures and lower pressures. It has to be kept in mind that the temperatures given are the temperatures of ions in front of the orifice, which could be totally different from the temperature of the neutral particles inside the orifice channel. Regarding this unknown temperature, the simple correction factor, which was higher in the low pressure case due to the worse orifice dimension ratio of $L/d = 2$, results in a very good correspondence with other measurement techniques and numerical simulation. Thus, the amount of recombination inside the orifice channel mainly depends on the length-to-diameter ratio of the given orifice.

To prove that the orifice correction factor was not necessary for the low-pressure conditions (despite the good results when calculating the local Mach number), the correction factor for the $L/d = 1$ orifice was applied to the data. This resulted in very high mole fractions of N and O. Carrying out the same calculation for this corrected particle distribution as already explained obviously leads to a lower mean molar mass, a lower mean number of DOFs, and correspondingly a lower Mach number. Additionally, the supersonic conditions would just be reached at $y = 80$ mm instead of 100 mm, while the stagnation pressure calculated behind the stationary shock front would be 0.36 mbar. Thus, agreement is worse when an orifice correction is applied.

With a modification of the orifice head, the mass spectrometer is now in a state where it is possible to investigate the erosion products of heat protection material placed directly in front of it. The spectrometer head will be reconstructed as a two-stage system with a skimmer for the detection of freestream plasma conditions at high pressures.

Acknowledgments

This work was performed under the auspices of the Sonderforschungsbereich 259 of the Deutsche Forschungsgemeinschaft. We wish to thank all our colleagues who were involved in the operation of the plasma wind tunnels and who supported and accompanied this work with advice and experimental and numerical results.

References

[1]Auweter-Kurtz, M., Habiger, H., Laure, S., Messerschmid, E., Röck, W., and Tubanos, N., "The IRS Plasma Wind Tunnels for the Investigation of Thermal Protection Materials for Reentry Vehicles," 1st European Symposium on Aerothermodynamics for Space Vehicles, ESTEC, Nordwijk, The Netherlands, May 1991.

[2]Schönemann, A., Auweter-Kurtz, M., Dabalà, P., Fasoulas, S., Früholz, H., Habiger, H., Kurtz, H., Laure, S., Loesener, O., and Röck, W., "The Plasma Wind Tunnels PWK1, PWK2," Inst. für Raumfahrtsysteme, Internal Rept., IRS 92-P6, Stuttgart, Germany, July 1992.

[3]Auweter-Kurtz, M., Habiger, H., Kurtz, H., Laure, S., Röck, W., and Tubanos, N., "Die Plasmawindkanäle PWK-IRS—Werkzeuge zur Untersuchung von Hitzeschutzmaterialien für Rückkehrfahrzeuge," *Zeitschrift für Flugwissenschaften*, Vol. 17, Springer-Verlag, Berlin, Feb. 1993, pp. 1–15.

[4]Laure, S., Auweter-Kurtz, M., Fasoulas, S., and Kurtz, H., "Reentry Simulation Within an Induction Heated Plasma Wind Tunnel," 2nd European Symposium on Aerothermodynamics for Space Vehicles, ESTEC, Noordwijk, The Netherlands, Nov. 1994.

[5]Laure, S., Auweter-Kurtz, M., Fasoulas, S., Habiger, H., and Röck, W., "The IRS Plasma Wind Tunnels as a Tool for the Investigation of Planetary Entry Missions," AIAA Paper 92-3886, July 1992.

[6]Scott, C. D., "Survey of Measurements of Flow Properties in Arcjets," *Journal of Thermophysics and Heat Transfer*, Vol. 7, No. 1, 1993, pp. 9–24.

[7]Lago, V., Schönemann, A., Lasgorceix, P., Buuron, A., and Dudeck, M., "Supersonic Plasma Jet Device for Testing Space Craft Materials," 2nd European Symposium on Aerothermodynamics for Space Vehicles, ESTEC, Noordwijk, The Netherlands, Nov. 1994.

[8]Fasoulas, S., Auweter-Kurtz, M., Habiger, H., Laure, S., and Sleziona, C., "Investigation of a Nitrogen Flow Within a Plasma Wind Tunnel," AIAA Paper 93-2817, July 1993.

[9]Fasoulas, S., Auweter-Kurtz, M., and Habiger, H., "Experimental Investigation of a Nitrogen High-Enthalpy Flow," *Journal of Thermophysics and Heat Transfer*, Vol. 8, No. 1, 1994, pp. 48–58.

[10]Habiger, H., Auweter-Kurtz, M., and Kurtz, H., "Electrostatic Probes for the Investigation of Arc-Driven Electric Propulsion Devices," 23rd International Electric Propulsion Conf., IEPC 93-124, Seattle, WA, Sept. 1993.

[11]Röck, W., Auweter-Kurtz, M., Habiger, H., Laure, S., Dabalà, P., and Früholz, H., "Experimental Simulation of the Entry of HUYGENS into the Titan Atmosphere for the Thermal Protection Qualification," 44th IAF—Congress, IAF-93-I.3.227, Graz, Austria, 1993.

[12]Habiger, H., Auweter-Kurtz, M., and Kurtz, H., "Investigation of Arc Jet Plumes with Fabry-Perot Interferometry," AIAA Paper 94-3300, June 1994.

[13]Batey, J. H., "Quadrupole Gas Analysers," *Vacuum*, Vol. 37, No. 8, 1987, pp. 659–668.

[14]Schönemann, A., Auweter-Kurtz, M., Habiger, H., Sleziona, C., and Stöckle, T., "Experimental and Numerical Investigation of the Influence of Argon Used as Protection Gas in a Reentry Simulation Device," AIAA Paper 93-2829, July 1993.

[15]Schönemann, A., "Massenspektrometrie zur Untersuchung lichtbogenbeheizter Plasmen im Niederdruck-Plasmawindkanal," Ph.D. Dissertation, Univ. Stuttgart, Inst. für Raumfahrtsysteme, Stuttgart, Germany, July 1994.

[16]Litzow, M. R., and Spalding, T. R., *Mass Spectrometry of Inorganic and Organometallic Compounds*, Elsevier, Amsterdam, 1973, Chap. 3.

[17]Helm, H., "The Transmission of a Sampling Orifice for Charged and Excited Particles in the Molecular Flow Range," *Plasmaphysik*, Vol. 11, No. 3, 1978, pp. 147–153.

[18]Wise, H., and Ablow, C. M., "Diffusion and Heterogeneous Reaction. I. The Dynamics of Radical Reactions," *Journal of Chemical Physics*, Vol. 29, No. 3, 1958, pp. 634–639.

[19]Wise, H., and Ablow, C. M., "Diffusion and Heterogeneous

Reaction. IV. Effects of Gas-Phase Reaction and Convective Flow," *Journal of Chemical Physics*, Vol. 35, No. 1, 1961, pp. 10–18.

[20]Bird, R. B., Stewart, W. E., and Lightfoot, E. N., *Transport Phenomena*, Wiley, New York, 1960, Chap. 16.

[21]Park, C., "Review of Chemical-Kinetic Problems of Future NASA Missions. I: Earth Entry," *Journal of Thermophysics and Heat Transfer*, Vol. 7, No. 3, 1993, pp. 385–398.

[22]Willey, R. J., and Blake, D. J., "Gas Composition Measurements in Arc Heated Flowfields via Mass Spectrometry," *Journal of Thermophysics and Heat Transfer*, Vol. 5, No. 2, 1991, pp. 150–156.

[23]Schönemann, A., and Auweter-Kurtz, M., "Characterization of Nitrogen and Air Plasma Flows by Mass Spectrometry," *ISPC 11, Proceedings of the 11th International Symposium on Plasma Chemistry*, Loughborough, England, UK, 1993, pp. 458–463.

[24]Riemann, K.-U., "The Bohm Criterion and Sheath Formation," *Journal of Physics D: Applied Physics*, Vol. 24, 1991, pp. 493–518.

[25]Fette, K., and Hesse, J., "Abschätzung der für die Ionenextraktion wichtigen Parameter der Raumladungsschicht," *Zeitschrift für Naturforschung*, Vol. 25A, 1970, pp. 518–524.

[26]Oertel, H., *Stossrohre*, Springer–Verlag, Wien, 1966.

[27]Schönemann, A., Auweter-Kurtz, M., Habiger, H., Sleziona, C., and Stöckle, T., "Analysis of the Argon Additive Influence on a Nitrogen Arcjet Flow," *Journal of Thermophysics and Heat Transfer*, Vol. 8, No. 3, 1994, pp. 466–472.